



ARCHIVES
of
FOUNDRY ENGINEERING

ISSN (2299-2944)
Volume 18
Issue 1/2018

93 – 98

DOI: 10.24425/118818

17/1



Published quarterly as the organ of the Foundry Commission of the Polish Academy of Sciences

Microstructural and Tribological Characterization of Aluminium Bronzes with Additions of Si and Cr

B.P. Pisarek ^{a,*}, B. Kowalski ^a, H. Atapek ^b, Ş. Polat ^b, T. Tüfekçi ^b

^a Lodz University of Technology Department of Materials Engineering and Production Systems, ul. Stefanowskiego 1/15, 90-924 Łódź, Poland

^b Department of Metallurgical and Materials Engineering, Kocaeli University, Umuttepe Campus 41380 Kocaeli, Turkey

*Corresponding author. E-mail address: boguslaw.pisarek@p.lodz.pl

Received 23.05.2017; accepted in revised form 21.08.2017

Abstract

The article presents the investigation results of the crystallization (performed by means of the TDA method) and the microstructure of complex aluminium bronzes with the content of 6% Al, 4% Fe and 4% Ni, as well as Si additions in the scope of 1–2% and Cr additions in the scope of 0.1–0.3%, which have not been simultaneously applied before. For the examined bronze, the following tests were performed: hardness HB, impact strength (KU₂). For bronze CuAl6Fe4Ni4Si2Cr0.3, characterizing in the highest hardness, wear tests were conducted with dry friction and the dry friction coefficient. The investigations carried out by means of the X-ray phase analysis demonstrated the following phases in the microstructure of this bronze: α_{Cu} , γ_2 and complex intermetallic phases based on iron silicide type Fe₃Si (M_3Si $M=\{Fe,Cr,\dots\}$). Compared to the normalized aluminium bronzes ($\mu=0.18-0.23$), the examined bronze characterizes in relatively low wear and lower friction coefficient during dry friction ($\mu=0.147\pm 0.016$).

Keywords: Innovative foundry technologies and materials, Wear resistant aluminium bronze, TDA method, Microstructure, Tribological properties

1. Introduction

Copper alloys, in which the main addition is aluminium, constitute a wide group of alloys called aluminium bronzes. These alloys are assigned for casting highly-loaded parts, working under corrosive conditions (sea water) and/or exposed to abrasive wear. Introducing such alloy additions as Ni, Fe, Mn, Si into the aluminium bronze provided the possibility to develop high-strength bronzes from the group: CuAl10Fe5Ni5 [1–4], CuAl10Fe4Ni [5,6], resistant to wear both in their raw state and after thermal treatment [7,8]. Also, investigations of the effect of

Cr and Ag additions on the tribological properties of bronze CuAl9Ni5Fe4Mn in the presence of sea water were conducted [9]. Complex aluminium bronzes with the content of about 10% Al, 5% Fe and 5% Ni and additions of Cr, Mo, W, Si and/or C characterize in high mechanical properties, which especially include high abrasive and adhesive wear resistance [10]. The introduced alloy additions affected the type of the crystallizing phases κ_i ($i=I, II, III, IV$) and the amount and size of precipitates, as well as changed the microhardness of phases: κ_i , α_{Cu} , and γ_2 . Increasing the concentration of these additions in the bronze contributes to an increase of the microstructure reinforcement –

increase of hardness HB, UTS (R_m), YS (R_{p0.2}) – by negatively affecting the impact strength as well as elongation (decrease) [11].

Figure 1 shows the effect of the mass concentration of Al in the aluminium bronze on its mechanical properties [12]. This results from the fact that, with the aluminium content in the bronze in the range of 5–8%, the latter maintains the highest impact strength.

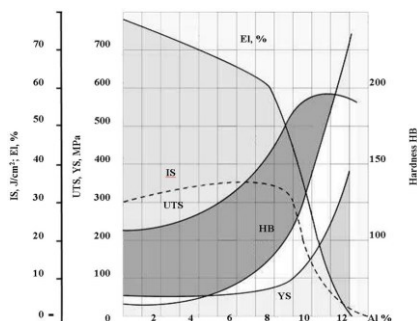


Fig. 1. Impact of Al on mechanical properties of aluminium bronzes [1]: IS – Impact Strength, J/cm²; EL – Elongation, %; UTS – Ultimate Tensile Strength, MPa; YS – Yield Strength, MPa

In the casting practice, according to BS EN 1982:2008 (previously existing standard BS 1400 1985), use are known only 4 types of aluminium bronzes with such a low weight concentration of aluminium, which are: CuAl5As, CuAl6Si2Fe, CuAl7Si2 and CuAl8Fe3. Among aluminium-silicon bronzes, high mechanical properties are exhibited by bronzes containing 6–8% Al and 1.5–3.0% Si [13]. It is estimated that 1% Si changes the structure and properties of Cu-Al alloys, similarly to 1.66% Al [14]. Silicon is mostly added to aluminium bronzes in the amount of 0.5–3.0% in order to improve the coefficient of sliding friction, and in consequence, to reduce the abrasive wear of these alloys. Fe and Ni additions introduced into aluminium bronzes are aimed at improving their mechanical and technological properties. The coefficient of dry friction μ of normalized bronzes Cu-Al-Fe and Cu-Al-Fe-Ni is within the scope of 0.18–0.23.

The innovative research presented in this article aimed at an analysis of the effect of a Cr and Si addition to aluminium bronze containing about 6% Al and about 4% Ni and Fe each on its microstructure and tribological properties. The analysis was based on the Box-Wilson method (Central Composite Design).

2. Methodology

In the investigations, constant mass concentrations of the elements were assumed: Al 6%, Fe 4%, Ni 4%. The content composition of up to 100% was obtained by a change in the Cu concentration in the bronze. The change in the chemical composition of the melts was obtained by a change in the weight concentration of Si and Cr, according to the assumed plan of a two-level experiment, which is presented in Table 1.

For the examined chemical compositions of the bronze, a thermal and derivative analysis (DTA) were performed on the TDA10PL tester.

Table 1.

Experimental design

x_i	Chemical composition, % wt.	
	Si	Cr
CenterPoint, x_i^0	1.5	0.2
Δx_i	0.5	0.1
Lower level $x_i^0 - \Delta x_i$	1.0	0.1
Upper level $x_i^0 + \Delta x_i$	2.0	0.3
E1	2.0	0.3
E2	2.0	0.1
E3	1.0	0.1
E4	1.0	0.3

The microstructure of the bronzes was observed on microsections cut out of casts in the DTA samples. The microsections were etched with the Klemm II reagent. Digital photographs of the bronzes were taken with the metallographic optical microscope Nikon Eclipse MA200.

For the identification of the chemical composition in the particular phases of the cast microstructure, the samples were observed under the scanning microscope Thermo Electro Corporation scanning microscope, with the accelerating voltage of 25 keV, equipped with an EDS analyzer.

The XRD phase analysis of alloy E1 was performed on the X'Pert PRO MPD PANalytical X-ray diffractometer.

The notched impact strength tests of the samples were conducted on a Charpy hammer, according to the standard PN-EN ISO 148 - 1:2010. For each bronze, impact strength measurements were performed on three test samples, which were prepared from perpendicular casts made in a sand mould prepared from fresh mass.

The tribological tests of the coefficient of dry friction were performed on the tribometer Nanovea type „Ball-on-Disc”. The tribological test samples were cut out of DTA casts. The parameters of the tribological tests are presented in Table 2.

Table 2.

Dry slipping conditions

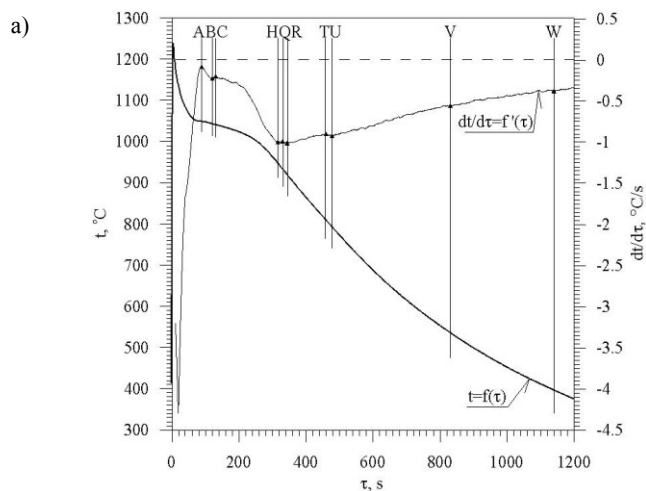
Load, N	Speed, m/s	Distance, m	Ball (counterpart)	Ball diameter, mm	Wear track radius, mm
10	0,05	100	100Cr6	5	3

3. Description of achieved results of own researches

3.1. General remarks

The decisive influence on the course of the crystallization process has the concentration of aluminium and silicon in the studied bronze. It can be inferred from the performed spectral analysis of the chemical composition of sample E1 that the latter

contains: Al 6.03%, Fe 3.80%, Ni 4.10%, Si 1.96%, Cr 0.30% and Mn 0.10%. Considering only the effect of Si on the shift of the characteristic lines of the Cu-Al phase equilibrium system, this alloy would go through a crystallization process close to that of bronze containing 9.28% Al (6.03% Al+1.66*1.96% Si), that is with a hypereutectic composition. Figure 2 shows the TDA characteristics of sample E1.



Point	τ , s	t , °C	$dt/d\tau$, °C/s
A	88	1019	-0.236
B	113	1012	-0.255
C	135	1007	-0.214
H	285	957	-0.549
Q	299	950	-0.486
R	382	892	-0.845
T	431	851	-0.827
U	460	827	-0.852
V	830	565	-0.555
W	1050	462	-0.423

b)

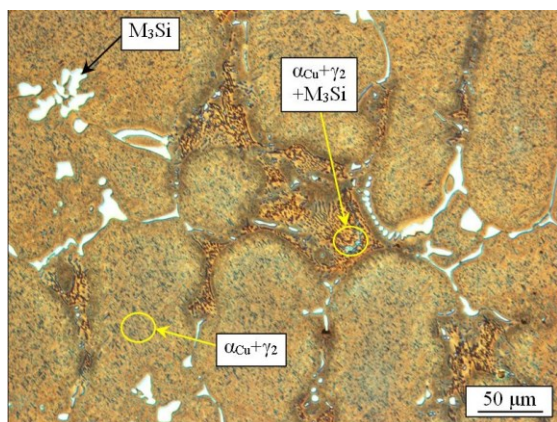


Fig. 2. Bronze CuAl6Fe4Ni4Si2Cr0.3 (E1):

a) TDA characteristics, b) microstructure: $\alpha_{Cu}+\gamma_2+M_3Si$

The analysis of the particular thermal effects was made based on the following:

- the TDA characteristics and the obtained microstructure (Fig. 1),
- the scope of the presence of phases on the phase equilibrium diagrams type Al-Cu-Si [15], Cu-Ni-Si [16], Cu-Fe-Si [17], Cu-Al-5%Fe-5%Ni [18], Fe-Si [19], in reference to the temperature of phase transformations and the component concentration,
- the results of the investigations of the element concentrations in the particular phases, shown in Figure 3,
- the results of the X-ray phase analysis, presented in Figure 4.

The crystallization process of complex aluminium bronze probably runs as follows: After the bronze has been overcooled below the equilibrium liquidus temperature, primary phase β nucleates and grows at the temperature $t_A=1018.5$ °C. Phase β , as a result of a relatively high alloy cooling rate, crystallizes metastably, strongly oversaturated with Ni, Cr, Fe and Si. The existing excess of these elements in respect of their solubility in phase β , is pushed in front of the crystallization front of this phase (L). From the liquid oversaturated with Ni, Cr, Fe and Si (L), eutectic $\alpha_{Cu}+\beta$ crystallizes at $t_C=1007.1$ °C. The eutectic phases also crystallize metastably as they are strongly oversaturated with these additions. With the lowering of the temperature as a result of the decreasing solubility of the additives, both from phase α_{Cu} and β , intermetallic phases precipitate in stages, rich in elements oversaturating them at $t_Q=950.4$ °C, and next at $t_T=850.7$ °C. With the lowering of the temperature of the bronze, at $t_V=565.3$ °C, a eutectoidal transformation $\beta \rightarrow \alpha + \gamma_2$ occurs. And so, on the derivation curve, the recorded thermal effects were caused probably by the crystallization of phases from the liquid alloy (L), or the phase systems formed as a result of the phase transformations in the solid state of:

- A-B – primary phase β of the solid solution with the electron phase matrix of the electron density of 3/2 – approximate formula: Cu_3Al , ($L \rightarrow L+\beta$),
- B-C-H – eutectic $\alpha_{Cu}+\beta$, ($L+\beta \rightarrow \beta+(\alpha_{Cu}+\beta)$),
- H-Q-R – complex non-equilibrium silicides, based on iron silicides type Fe_3Si (α_1) and Fe_2Si (α_2), ($\beta+(\alpha_{Cu}+\beta) \rightarrow \beta+(\alpha_{Cu}+\beta)+\alpha_1+\alpha_2$),
- R-T-U – decomposition of complex silicides type α_2 into complex silicides type α_1 , ($\beta+(\alpha_{Cu}+\beta)+\alpha_1+\alpha_2 \rightarrow \beta+(\alpha_{Cu}+\beta)+\alpha_1$),
- U-V-W – eutectoidal decomposition of phase β into eutectoid $\alpha_{Cu}+\gamma_2$, where γ_2 is the primary solid solution with the electron phase matrix of the electron density of 21/13 – approximate formula: Cu_9Al_4 , ($\beta+(\alpha_{Cu}+\beta)+\alpha_1 \rightarrow \alpha_{Cu}+\gamma_2+\alpha_1$).

The distribution of the secondary electron energy and the results of the local analysis of the chemical composition or from the marked area of the microstructure of bronze E1 (CuAl6Fe4Ni4Si2Cr0.3 Fig. 3), observed under the electron microscope, are presented in 4 a–d.

It can be inferred from the tests of the secondary electron energy distribution that in area 1, the chemical composition analysis results correspond probably to the eutectoidal mixture $\alpha_{Cu}+\gamma_2$ (Fig. 4d). In the Cu-Al equilibrium system, this transformation takes place at 565 °C, and on the DTA characteristics of the examined bronze, a transformation at $t_V=565.3$ °C was recorded

(Fig. 2). For alloy E1, this transformation occurs with low intensity and for a relatively long period of time $\tau_U - \tau_W$.

Intermetallic phases rich in Ni, Cr, Fe and Si precipitate in the interdendritic spaces of phase β (Fig. 1). Their shape is close to that of a rosette and they characterize in relatively large sizes (10–50 μm , point: 2, 3 and 4 Fig. 3). In turn, in the area of the crystallization of eutectic $\alpha_{Cu} + \beta$ (Fig. 2), the intermetallic phases characterize in a dominant lamellar structure and are much smaller than the previous ones (point 5 Fig. 3).

It can be inferred from the tests of the secondary electron energy distribution that, in points 2 and 5 (Fig. 4 b,c), the results of the analysis of the chemical composition correspond to complex iron silicides. The ratio of the atomic concentrations of only the elements Fe/Si in points 2 (Fig. 4c) equals 2,63/1, and in point 5 (Fig. 4d), it equals 2,42/1. One can presume in the analysis of these proportions that, in the microstructure of the examined bronze, complex iron silicides (M_3Si) based on silicide Fe_3Si (α_1) have been probably formed.

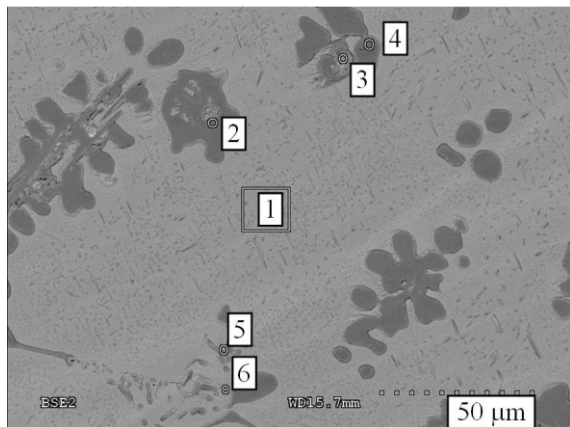


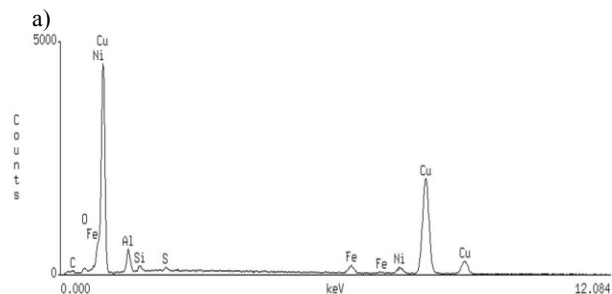
Fig. 3. Bronze $CuAl_6Fe_4Ni_4Si_2Cr_{0,3}$ (E1), microstructure observed under an electron microscope

The tests of the secondary electron energy distribution suggest that, in point 6, the chemical composition analysis results correspond to the solution α_{Cu} (Fig. 4d). The atomic concentrations of the additions of Ni, Al, Si and Fe do not exceed their maximal solubility in copper, which is as follows: Ni 100% at. (100% wt.), Al 19.6% at. (9.38% wt.), Si 11.25% at. (5.31% wt.) and Fe 4.5% at. (3.98% wt.).

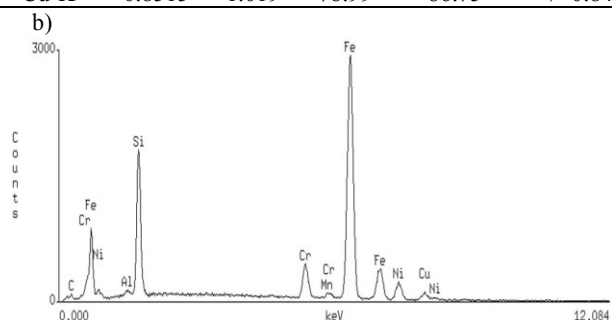
On the XRD (anode Cu: $CuK - 1.5406 \text{ \AA}$) X-ray diffraction pattern (Fig. 5), the following phases were identified in the bronze microstructure: Cu (α_{Cu}), Cu_9Al_4 (γ_2), Fe_3Si (α_1). No phase for which the effect denoted as „*” occurs, was identified ($2\theta=78^\circ$). Finding a solution to this problem constitutes a challenge in respect of further investigations.

Table 3 and Figure 6 show: mean values of hardness HB, impact strength (KU_2) and their standard deviations s_{HB} and s_{KU_2} . It can be inferred from the presented data that bronze $CuAl_6Fe_4Ni_4Si_2Cr_{0,3}$ characterizes in the highest hardness ($183 \pm 1.7 \text{ HB}$) and the lowest impact strength (which is still relatively high: $KU_2 = 21.1 \pm 2.94 \text{ J/cm}^2$).

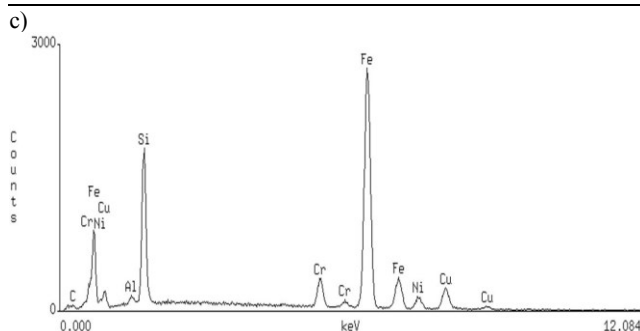
Figure 7 and 8 show: the wear area of sample $CuAl_6Fe_4Ni_4Si_2Cr_{0,3}$ (E1) during dry abrasion and the change of the friction coefficient μ .



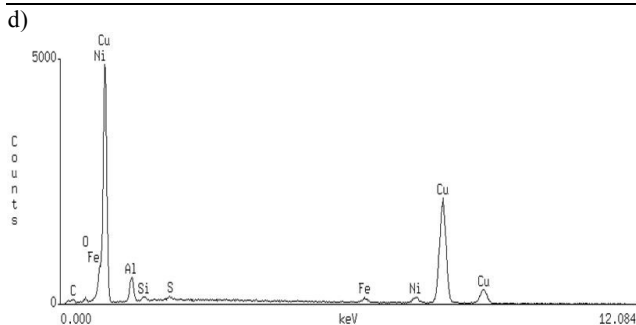
Element	k-ratio (calc.)	ZAF	Atom., %	Element Wt., %	Wt. % Err., (1-Sigma)
Al-K	0.0165	3.328	11.80	5.50	+/- 0.13
Si-K	0.0040	2.439	2.00	0.97	+/- 0.06
S-K	0.0032	1.534	0.88	0.49	+/- 0.05
Fe-K	0.0328	0.815	2.77	2.68	+/- 0.19
Ni-K	0.0371	0.973	3.56	3.62	+/- 0.32
Cu-K	0.8515	1.019	78.99	86.75	+/- 0.84



Element	k-ratio (calc.)	ZAF	Atom. %	Element Wt. %	Wt. % Err., (1-Sigma)
Al-K	0.0018	2.584	0.84	0.46	+/- 0.05
Si-K	0.0705	1.889	23.38	13.32	+/- 0.14
Cr-K	0.0661	0.882	5.53	5.84	+/- 0.10
Fe-K	0.6794	1.024	61.39	69.57	+/- 0.54
Ni-K	0.0621	1.112	5.79	6.90	+/- 0.39
Cu-K	0.0311	1.145	2.76	3.56	+/- 0.41
Mn-K	0.0034	1.041	0.32	0.36	+/- 0.11



Element	k-ratio (calc.)	ZAF	Atom. %	Element Wt. %	Wt. % Err., (1- Sigma)
Al-K	0.0025	2.628	1.20	0.66	+/- 0.06
Si-K	0.0703	1.920	23.81	13.50	+/- 0.13
Cr-K	0.0534	0.888	4.52	4.74	+/- 0.16
Fe-K	0.6399	1.015	57.58	64.93	+/- 0.52
Ni-K	0.0418	1.102	3.89	4.61	+/- 0.37
Cu-K	0.1018	1.135	9.01	11.56	+/- 0.49



Element	k-ratio (calc.)	ZAF	Atom. %	Element Wt. %	Wt. % Err., (1- Sigma)
Al-K	0.0176	3.336	12.59	5.87	+/- 0.13
Si-K	0.0031	2.452	1.55	0.75	+/- 0.06
S-K	0.0028	1.537	0.79	0.44	+/- 0.05
Fe-K	0.0167	0.809	1.40	1.35	+/- 0.18
Ni-K	0.0337	0.971	3.23	3.28	+/- 0.31
Cu-K	0.8686	1.017	80.45	88.32	+/- 0.85

Fig. 4. Distribution of secondary electron energy and results of the local analysis of the chemical composition or in the marked area of the microstructure of bronze E1 (CuAl6Fe4Ni4Si2Cr0.3 Fig.

2), observed under an electron microscope:

a) area 1, b) point 2, c) point 5, d) point 6

It can be inferred from the presented images taken both with use means of the optical and electron microscope stated that the basic wear mechanism is adhesive wear (visible pulling out of material along the abrasion path). The tested alloy is characterized by its short run-in period (40 m) and then reached to a steady-state. Although alloy had a highest HB hardness value (Tab. 3), it suffered from friction. The wear of sample CuAl6Fe4Ni4Si2Cr0.3 (E1) in the dry abrasion process was at the level of $3.56 \cdot 10^{-4} \text{ mm}^3/\text{N} \cdot \text{m}$ (mass loss of the sample: $3.56 \cdot 10^{-1} \text{ mm}^3$). Initial tribological tests were carried out to determine the variation of friction coefficient values as a function of sliding distance. The mean value of coefficient of dry friction equals $\mu=0.147 \pm 0.016$. The low value of this coefficient is probably due to the presence of hard silicides in fine-grained eutectoid matrix (Fig. 2b, Fig. 3).

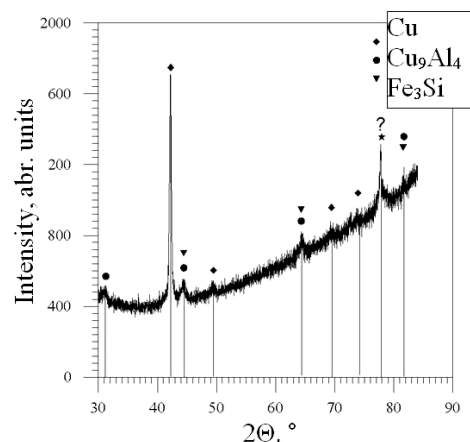


Fig. 5. X-ray diffraction pattern of bronze E1

Table 3. Mean values of hardness HB, impact strength (KU₂) and their standard deviations sHB and sKU₂

Alloy	HB	sHB	KU ₂ , J/cm ²	sKU ₂ , J/cm ²
CuAl6Fe4Ni4Si1Cr0.1	164	0.3	64.3	3.35
CuAl6Fe4Ni4Si2Cr0.1	178	2.5	43.7	2.47
CuAl6Fe4Ni4Si1.5Cr0.2	180	1.2	59.4	5.16
CuAl6Fe4Ni4Si1Cr0.3	165	1.0	59.8	5.89
CuAl6Fe4Ni4Si2Cr0.3	183	1.7	21.1	2.94

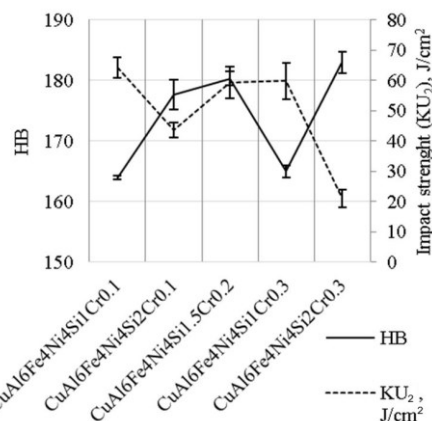


Fig. 6. Mean values of hardness HB impact strength KU₂ and their standard deviations for the tested bronze

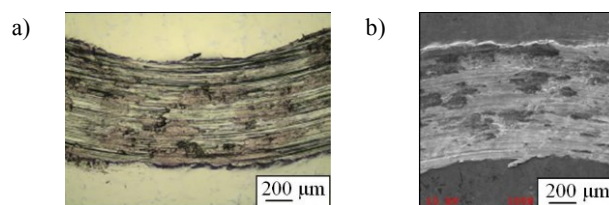


Fig. 7. Wear area of sample CuAl6Fe4Ni4Si2Cr0.3 (E1):
a) optical microscope, b) electron microscope

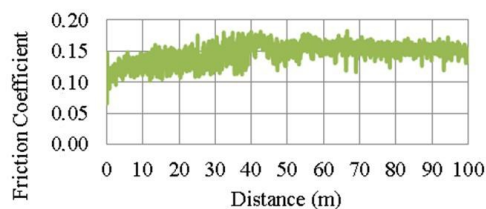


Fig. 8. Change of the friction coefficient μ of sample CuAl6Fe4Ni4Si2Cr0.3 (E1) during dry friction

4. Conclusions

It can be concluded from the presented studies that bronze CuAl6Fe4Ni4Si2Cr0.3, compared to the normalized aluminium bronzes containing about 6% Al, 4% Fe and 4% Ni characterizes in high mechanical and performance properties: high hardness $HB=183\pm 1.7$, impact strength (KU_2) of about 21.1 ± 2.94 J/cm², dry abrasion wear resistance of about $3.56\cdot 10^{-4}$ mm³/N·m, and coefficient of dry friction μ of about 0.147 ± 0.016 . The low value of this coefficient is probably due to the presence of hard silicides in fine-grained eutectoid matrix

References

- [1] Shi, Z., Sun, Y., Bloyce, A. & Bell, T. (1996). Unlubricated rolling-sliding wear mechanisms of complex aluminium bronze against steel. *Wear*. 193, 235-241.
- [2] Lv, Y., Wang, L., Xu, X., Han, Y. & Lu, W. (2015). Investigation of the Microstructure and Corrosion Properties of Friction Stir Processed Cast NiAl Bronze. *Materials Transactions*. 56(9), 1523-1529.
- [3] Thapliyal, S. & Dwivedi, D.K. (2016). Study of the effect of friction stir processing of the sliding wear behavior of cast NiAl bronze: A statistical analysis. *Tribology International*. 97, 124-135.
- [4] Alam, S., Marshall, R.I. & Sasaki, S. (1996). Metallurgical and tribological investigations of aluminium bronze bushes made by a novel centrifugal casting technique. *Tribology International*. 29(6), 487-492.
- [5] Li, Y., Ngai, T.L. & Xia, W. (1996). Mechanical friction and wear behaviours of a novel high-strength wear-resisting aluminum bronze. *Wear*. 197, 130-136.
- [6] Prasad, B.K. (2004). Sliding wear behaviour of bronzes under varying material composition, microstructure and test conditions. *Wear*. 257, 110-123.
- [7] Shi, Z., Sun, Y., Bloyce, A. & Bell, T. (1996). Influence of surface melting on dry rolling-sliding wear of aluminium bronze against steel. *Wear*. 198, 300-306.
- [8] Yaşara, M. & Altunpak, Y. (2009). The effect of aging heat treatment on the sliding wear behaviour of Cu–Al–Fe alloys. *Materials and Design*. 30, 878-884.
- [9] Jin, K., Qiao, Z., Zhu, S., Cheng, J., Yin, B. & Yanga, J. (2016). Synthesis effects of Cr and Ag on the tribological properties of Cu-9Al-5Ni-4Fe-Mn bronze under seawater condition. *Tribology International*. 101, 69-80.
- [10] Pisarek, B.P. (2008). Abrasive wear of BA1055 bronze with additives of Si, Cr, Mo and/or W. *Archives of Foundry Engineering*. 8(3), 209-216.
- [11] Pisarek, B. (2013). Aluminium bronzes with additions of Cr, Mo and/or W with high resistance to wear. *Zeszyty Naukowe Nr 1141. Rozprawy Naukowe Z. 441*. Łódź: Wydawnictwo Politechniki Łódzkiej. (in Polish).
- [12] Górny, Z., Lech, Z., Rutkowski, K., Strojny, Z., Welkens, T. (1963). *Foundry alloys of non-ferrous metals. Melting and casting technology*. Warszawa: WNT. (in Polish).
- [13] Adamski, Cz., Bonderek, Z., Piwowarczyk, T. (1972). *Microstructure of cast alloys of copper and zinc*. Katowice: Śląsk. (in Polish).
- [14] Górny, Z., Sobczak, J. (2005). *Modern molding materials based on non-ferrous metals*. Kraków: ZA-PIS. (in Polish).
- [15] Raghavan, V. (2007). Al-Cu-Si (Aluminum-Copper-Silicon). *Journal of Phase Equilibria and Diffusion*. 28(2), 180-182. <https://doi.org/10.1007/s11669-007-9024-y>.
- [16] Wang, C., Zhu, J., Lu, Y., Guo, Y. & Liu, X. (2014). Thermodynamic description of the Cu-Ni-Si system. *Journal of Phase Equilibria and Diffusion*. 35(1), 93-104. <https://doi.org/10.1007/s11669-013-0277-3>.
- [17] Raghavan, V. (2010). Cu-Fe-Si (Copper-Iron-Silicon). *Journal of Phase Equilibria and Diffusion*. 31(2), 169-171. <https://doi.org/10.1007/s11669-010-9647-2>.
- [18] Brezina, P. (1973). Gefügeumwandlungen und mechanische Eigenschaften der Mehrstoff-Aluminiumbronzes vom Typ CuAl 10 Fe5 Ni5. *Giesserei-Forschung*. 25(3), 1-10.
- [19] Massalski, T.B., Okamoto, H., Subramanian, P.R. & Kacprzak, L. (1990). *Binary Alloy Phase Diagrams*, 2nd ed., (eds. T.B. Massalski, J. L. Murray, L. H. Bennet, H. Baker), ASM International.